Diagnostics of the Extratropics

John Methven

Department of Meteorology, University of Reading,
Reading, RG6 6BB, United Kingdom
J.Methven@reading.ac.uk

ABSTRACT

Diagnostics quantify properties of the atmosphere from information on its current state and recent history. They often involve equations relating different variables at one instant. The most powerful diagnostics are those which relate to conceptual and theoretical models for the evolution of the atmosphere. They enable us to anticipate what will happen next before explicit calculation of a forecast, and to identify "unphysical behaviour" or other model failings. This talk addresses three features that make atmospheric behaviour non-local and which makes the design of useful diagnostics difficult: (i) long-range transport of tracers, (ii) balance between variables giving rise to action-at-a-distance and (iii) the lack of scale separation between the "background flow" and "eddies".

1 Introduction

Accurate weather predictions would be impossible without detailed numerical models. The dynamical core of these models is based on numerical representation of a few partial differential equations that have been known for over a century. Nevertheless, solutions of these equations are unknown except in very special circumstances and a rich zoo of phenomena are supported.

Even in kinematic problems where the wind field is taken as given, the trajectories of fluid parcels (or air-masses) are chaotic. While steady horizontal flow in a single layer is not chaotic, only weak time dependence or three-dimensionality to the flow is required for trajectories to be non-integrable and chaotic behaviour, characterised by sensitivity to initial conditions. To make matters worse the solutions of the dynamical equations (stemming from conservation of mass, momentum and entropy) are themselves chaotic. This behaviour gives rise to the first problem addressed here - the complex pathways for transport of materially conserved properties such as (potential) temperature and trace constituents. In Sections 2.3 and 2.4, particular attention is given to the transport of water vapour, given its central importance to weather and climate.

This talk will focus on weather forecasting timescales from 1-15 days and the large-scale phenomena that dominate them. The second issue arising are strong constraints associated with balance between variables. At leading order static relationships include hydrostatic and geostrophic balance and their combination in thermal wind balance. Evolution can only be described at next order which involves time derivatives. The quasi-geostrophic system provides a consistent view of mid-latitude dynamics enabling some form of prediction. It contains the essence of more sophisticated definitions of balanced flow. The cornerstone of the theory is quasi-geostrophic potential vorticity (PV). It is materially conserved following the geostrophic flow (along pressure levels). Furthermore, the flow and temperature field can be deduced from the distribution of PV alone (and potential temperature on the boundaries) through inversion of a differential operator defining PV in terms of gradients of geostrophic variables. The use of these ideas in the diagnosis of the much more complex numerical weather prediction (NWP) models is discussed in Section 3 including: attribution of changes in PV along trajectories to different physical processes, PV error diagnostics and the use of piecewise PV inversion to modify forecasts.

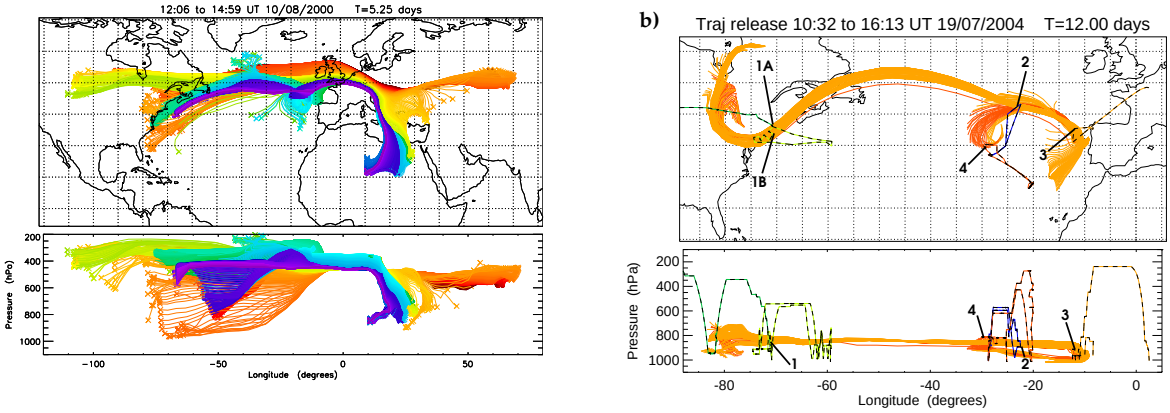

Figure 1: Air mass trajectories back and forwards from flight tracks. a) Flight on 15/8/00 over Germany and b) flight (#2) from the Azores 19/7/04 during the ITCT-Lagrangian experiment. Labels 1, 3 and 4 indicate flights which were shown to intercept the same air mass on the basis of matching trajectories and hydrocarbon fingerprints (from Methven et al. 2006).

The third issue arises from attempts to relate atmospheric behaviour to a notional partition between a "slowly evolving background state" and disturbances to it: an essential ingredient of most atmospheric theories. In Section 4, the difficulties with defining a suitable background are discussed. Once defined it is possible to derive wave activity conservation laws. The wave activity flux can be related to the group velocity of Rossby wave packets. Some examples of how stationary Rossby waves relate to teleconnection patterns and the occurrence of persistent weather are explored. Finally, it is acknowledged that many phenomena are related to coherent structures rather than waves. The latest uses of feature tracking to describe the statistics of stormtracks, their structures and predictability are briefly described.

2 Transport Diagnostics

2.1 Trajectory calculations and their accuracy

Atmospheric flow is three-dimensional and time varying and as a result air parcel trajectories are sensitive to initial conditions, such that neighbouring parcels separate exponentially on average. Such behaviour is referred to as chaotic advection. For example, Fig. 1a illustrates trajectories calculated forwards and backwards in time from a segment of aircraft flight track over Germany. Not only is the sampled air destined to separate rapidly downstream, but the back trajectories indicate that the air originates from a wide area. This behaviour is particularly important for the chemical composition of the atmosphere. Air masses can be carried many thousands of kilometres by the flow while retaining a composition distinct from their surroundings because photochemistry of many species and mixing between air masses takes days or even weeks. As a result, to observe the chemical evolution of an air mass it is necessary to monitor it over many days while it travels thousands of kilometres.

This motivated the ITCT-Lagrangian Experiment which took place within the framework of the ICARTT campaign in summer 2004 (Fehsenfeld 2006). Polluted air masses were sampled on leaving the continental boundary layer over the USA (e.g., flight 1 in Fig. 1b) and intercepted again several times en route across the Atlantic Ocean. Five cases of trans-Atlantic transport with 3 or more aircraft interceptions were verified during a 3 week period (Methven *et al.* 2006). Did the aircraft really sample the same air mass many times? This question was addressed by matching the multi-component hydrocarbon finger-

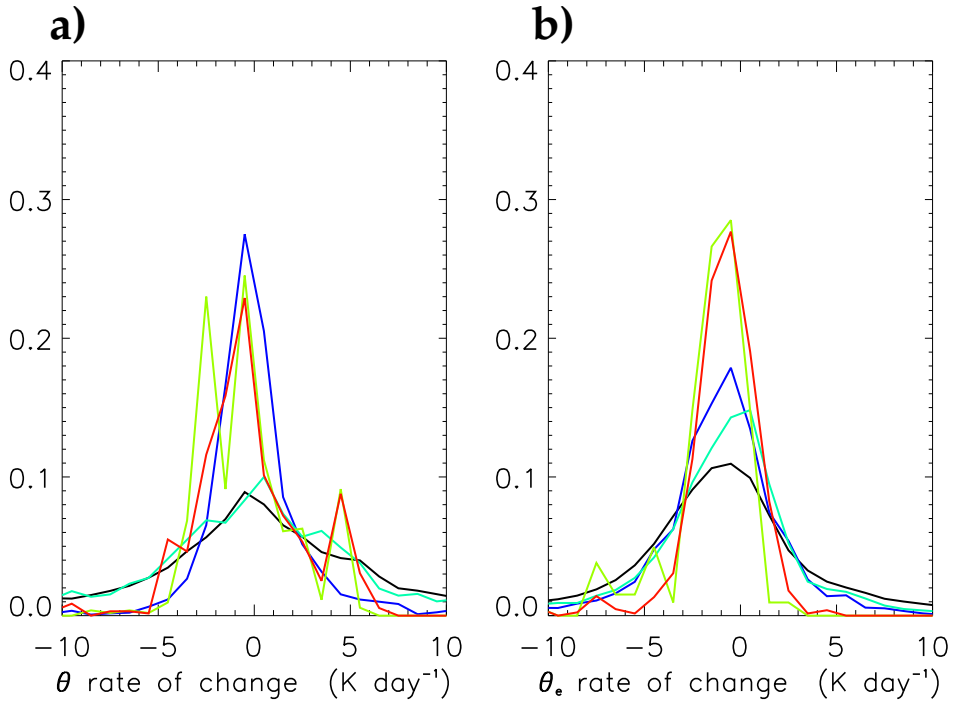

Figure 2: Rate of change in θ and θ_e following air masses, as inferred from interceptions of the air masses by different aircraft during the five ITCT-Lagrangian cases. Black *obtained through random pairing of flight intervals with hydrocarbon samples,* dark green *from matching hydrocarbon samples,* blue *from pairs with trajectory matches (but not considering hydrocarbons) and* red *coincident matches between hydrocarbon samples and trajectories.*

print of bottle samples collected by the 4 aircraft involved and then seeking the subset of matching pairs that were linked by trajectories shadowing one another closely moving backwards and forwards in time from the two samples. The quality of the matches was evaluated with independent observations of temperature and humidity from the matching flight segments. Figure 2 shows histograms of the difference in potential temperature (θ) and equivalent potential temperature (θ_e) between any two matching samples divided by the time elapsed between them. Coincident matches obtained by two Lagrangian models are peaked much more strongly near zero (red and green) than obtained by pairing random samples (black), as would be expected by almost adiabatic transport. Note that $D\theta/Dt$ has a secondary peak at 5 K day^{-1} resulting from polluted air that experienced latent heat release during ascent. θ_e is materially conserved during this process and so the positive peak is not seen.

Photochemical models simulating the changing composition following air masses tie in closely with the aircraft data. For example, the red trajectories in Fig. 3 link the interceptions and clearly model ozone agrees with the observations to within the variability of the air mass. Carbon monoxide is systematically over-estimated downstream by the model which can be attributed to the representation of mixing with cleaner air aloft.

In all the figures shown, trajectories are calculated by numerical integration of $D\mathbf{x}/Dt = \mathbf{u}(\mathbf{x},t)$ using a 4th order Runge-Kutta algorithm and interpolating winds from ECMWF operational analyses in both time and space to air parcel locations. Therefore, the consistency between the calculated trajectories and the multi-variate observations is a testament to the quality of the analysed wind fields. The close conservation of θ_e indicates that the temperature and humidity interpolated to trajectory points are also consistent. Furthermore, it was only possible to guide aircraft to interception points spaced across the Atlantic because trajectories derived from forecast winds were sufficiently accurate. Even the aircraft

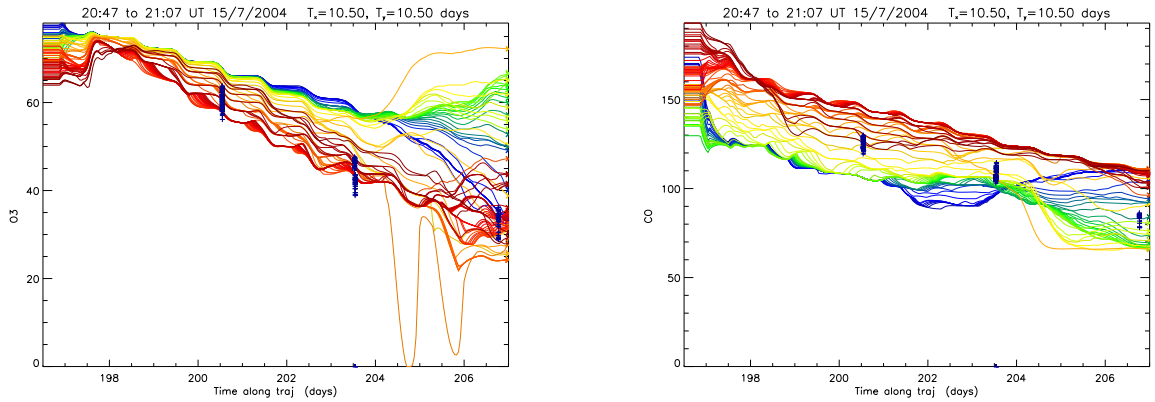

Figure 3: Simulation of chemical composition for an ensemble of air masses initialised from a segment of flight track downwind of New England, USA. a) Ozone and b) carbon monoxide. Crosses indicate observations during interceptions 2, 3 and 4 across the Atlantic (as shown in Fig. 1b).

closest to the USA flew in polluted air that was forecast to pass within range of the Azores, France or both.

Why are trajectory calculations so accurate? In part, it is because the winds are dominated by large-scale flow related to Rossby waves and baroclinic weather systems due to the scale-effect of potential vorticity (PV) inversion (Hoskins *et al.* 1985): given two waves with equal PV amplitude but different scales, the longer wave will have a greater influence on the fluid velocity. In addition, and perhaps counter-intuitively, chaotic advection helps here. The rapid separation of trajectories results in an exponential rate of stretching and thinning of air masses with distinct composition. Consequently we can simulate structure in tracer fields (e.g., ozone) accurately on scales at least 6 times smaller than the smallest resolved scale in the wind fields (Methven and Hoskins 1999). Here an accurate tracer simulation is defined as one where the displacement error of a filament is less than its width (as with resolution of two objects in optics). Note that trajectory error will typically be much greater in the direction along tracer filaments, but the composition varies much more slowly in that direction.

2.2 Reverse domain filling trajectory calculations reveal finescale structure

Stirring by chaotic advection results in stretching and folding of long-lived tracers and the so-called "cascade" in tracer towards smaller scales. In order to achieve some form of statistical equilibrium distribution, tracer contrasts must be maintained by non-conservative processes on the largest scales. For example, there is a large specific humidity decrease from equator to pole associated with the dependence of saturation vapour pressure on temperature; sub-saturated specific humidity is conserved following air masses, but on moving to colder areas (upwards and polewards) the air saturates, water vapour condenses and specific humidity decreases accordingly. The corollary to the cascade is that back trajectories of air parcels, if followed for long enough, must hark from disparate origins with very different characteristic composition. This notion led to the *reverse domain filling* trajectory technique (e.g., Sutton *et al.* 1994) where trajectories are calculated backwards in time from a finescale grid. Tracer values at the origins of those trajectories are estimated from a large-scale distribution and *attributed* to the trajectory and its arrival point on the grid. Figure 4 shows an example of an RDF reconstruction of specific humidity on a level and section through a 3D domain (Methven *et al.* 2003). Clearly the RDF3D technique represents a dry intrusion seen in Meteosat satellite imagery with a high degree of fidelity, and that this long, thin

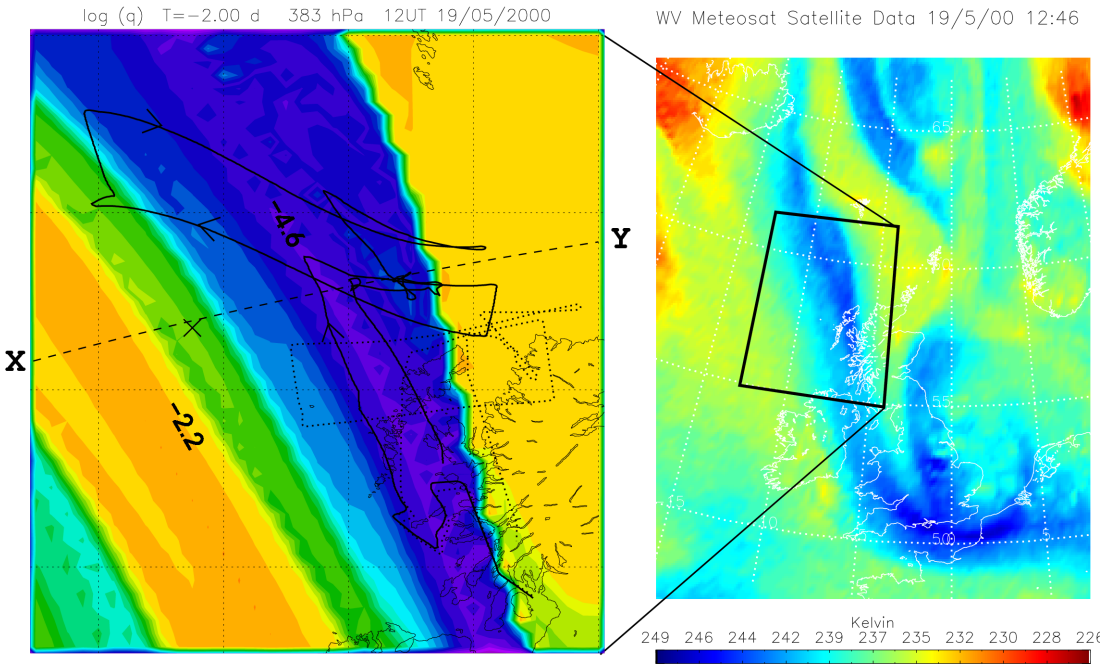

Figure 4: Finescale structure in specific humidity reconstructed using reverse domain filling (RDF) back trajectories and its comparison with a water vapour channel satellite image. [from Methven et al. 2003].

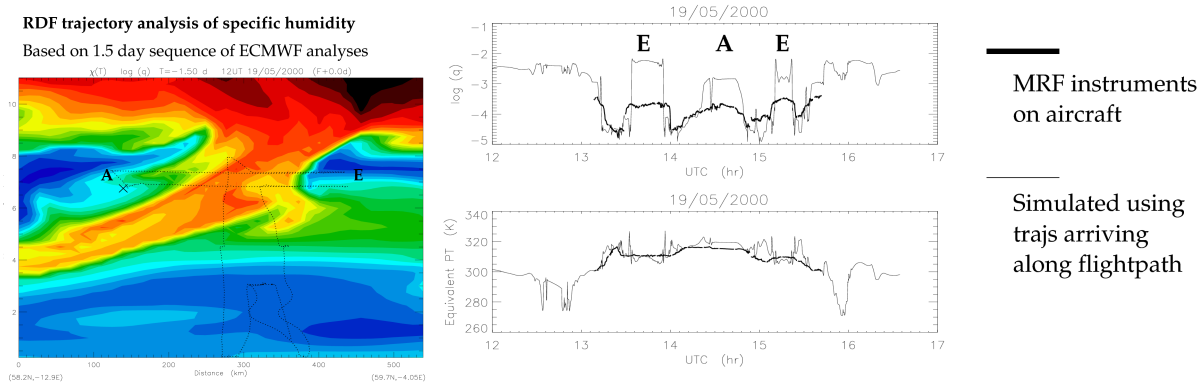

Figure 5: a) Cross-section across the dry intrusion of Fig. 4 showing a tropopause fold sloping down to the west and the flight track of the Met Research Flight C130 aircraft. b) Comparing reconstructed specific humidity and equivalent potential temperature with flight data.

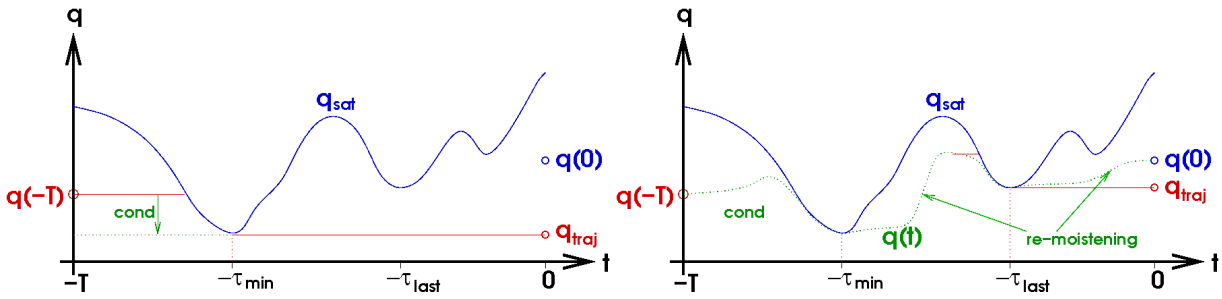

Figure 6: Depictions of two assumptions made in advection-condensation models. (Left) the Lagrangian cold point determines the arrival mixing ratio ($q_{traj} = min(q_{sat})$). (Right) mixing ratio from the last condensation event, identified along the trajectory using analyses, is carried to the arrival point.

intrusion is associated with a sloping tropopause fold in cross-section.

Again we could ask whether the finescale structure was accurately represented. Figure 5b shows evidence from an aircraft flight through the fold that θ_e is simulated to within a few K, although clearly specific humidity at the origin of the saturated air masses is far higher than observed by the aircraft. The θ_e correspondence indicates that the decrease in specific humidity can be attributed to condensation during resolved ascent. Evidence from many case studies shows that back trajectories stretching 1 to 4 days backwards are best for simulating the finescale structure observed by in situ or remote sensing in the mid-latitudes. Shorter trajectories do not go far enough to pick out the tracer gradients between air masses while longer ones reproduce structures on finer scales than observed (Balluch and Haynes 1997), indicating that non-conservative processes, especially mixing, act to eliminate these smaller scales. Arnold *et al.* (2007) estimated that the exponential turbulent diffusion timescale associated with the air masses tracked during the ITCT-Lagrangian experiment was as much as 10 days in conditions with almost no ascent above the boundary layer. In general, close to dynamically active features such as fronts and tropopause folds mixing is faster than this, whether by entry into the boundary layer or turbulence associated with strong shear or convection.

2.3 Allowing for non-conservation: Advection-condensation models for water vapour

Transport is particularly important for the distribution of water throughout the atmosphere. When air is sub-saturated, water vapour mixing ratio is materially conserved (carried as a tracer). However, if an air mass experiences colder temperature which has a lower saturation vapour pressure it will become saturated. Super-saturation is possible but typically condensation occurs. This information is the physical basis of simple *advection-condensation* models where the history of water vapour is simulated along trajectories (e.g., Sherwood 1996; Pierrehumbert and Roca 1998).

In most advection-condensation models, the minimum saturation mixing ratio along the entire trajectory is sought and it is assumed that the air mass retains this value from then on (Fig. 6a). Since saturation vapour pressure is a function of temperature alone, this is referred to as the humidity determined by the *Lagrangian cold point*. Fueglistaler *et al.* (2005) have shown how the stratospheric humidity distribution is largely determined by the Lagrangian cold point of air entering through the tropical tropopause and its subsequent advection. This method works well for that problem because the tropical tropopause (especially near Indonesia) is much colder than the rest of the stratosphere and the majority of air passes through this "stratospheric fountain" location on entry into the straosphere (Newell and Gould-Stewart 1981). Therefore, the stratosphere is well below saturation and one does not need to consider later condensation events. However, tropospheric air masses experience re-moistening associated with mixing.

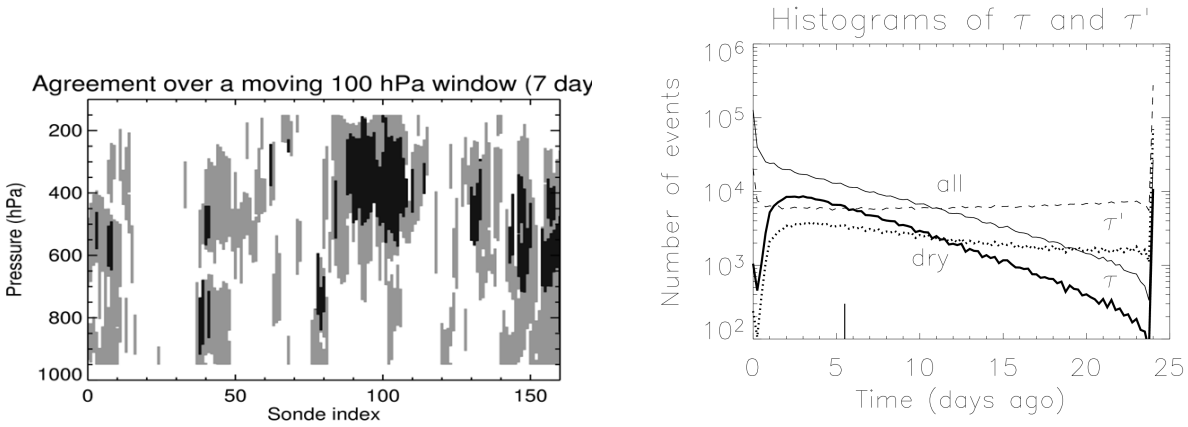

Figure 7: Results derived using advection-condensation models along trajectories. a) Black shading shows dry layers (RH< 20%) observed by sondes from above the West Pacific, grey shows dry layers from the model that are not seen in observations (Cau et al. 2005). b) Histograms of the time since last condensation events for air arriving dry in the subtropics and tropics (Cau et al. 2007). Dashed line shows time since the Lagrangian cold point for all trajectories. Bold line shows time since last condensation for dry air masses, allowing for re-moistening after the Lagrangian cold point.

Frequently, this occurs within the boundary layer which is in contact with the Earth's surface and the humidity fluxes from it, although it may occur above the boundary layer, for example by mixing with air ascending in convective updrafts. Cau *et al.* (2007) devised a modification to the basic advection-condensation model which is more appropriate for following tropospheric air masses. Both humidity mixing ratio and temperature are interpolated from analyses to trajectory points and the last event when saturation reduces the mixing ratio is assigned as the trajectory humidity q_{traj} (Fig. 6b). This allows for re-moistening implicit in the history of the analyses since the Lagrangian cold point and subsequent condensation events. Note that q_{traj} still differs from the analysis at arrival time, partly because the finite resolution of the analysis grid results in an unrealistically rapid rate of mixing with moister air as dry air masses stretch and thin through chaotic advection.

Back trajectory reconstruction of the humidity field works surprisingly well even in the deep tropics, where the large-scale flow is not well approximated by geostrophic balance. Figure 7a (from Cau *et al.* 2005) compares dry layers observed on radiosonde profiles from Kapingamarangi, one of the TOGA COARE stations in the tropical West Pacific, with the trajectory simulation. All observed dry layers (black shading) are picked up by the model, but the model indicates many more dry layers that are not observed (grey). This is because the Lagrangian cold point assumption was used and the lack of re-moistening results in a dry bias which increases with trajectory length.

2.4 Trajectory statistics: Density of origin

We have seen that trajectory calculations driven using ECMWF analyses are accurate across the globe. It is tempting to use them to diagnose the general circulation of the atmosphere from a Lagrangian perspective and its implications for the water vapour distribution. However, ensembles of trajectory diverge rapidly, even if from the small starting volumes shown in Fig, 1a. If trajectories are released from a wide area or multiple levels they rapidly form a tangle that is very difficult to visualise, let alone analyse quantitatively.

One approach is to identify particular events along trajectories, such as the last condensation, and create number density distributions summarising the location of events. For example, Jackson *et al.* (2001) used

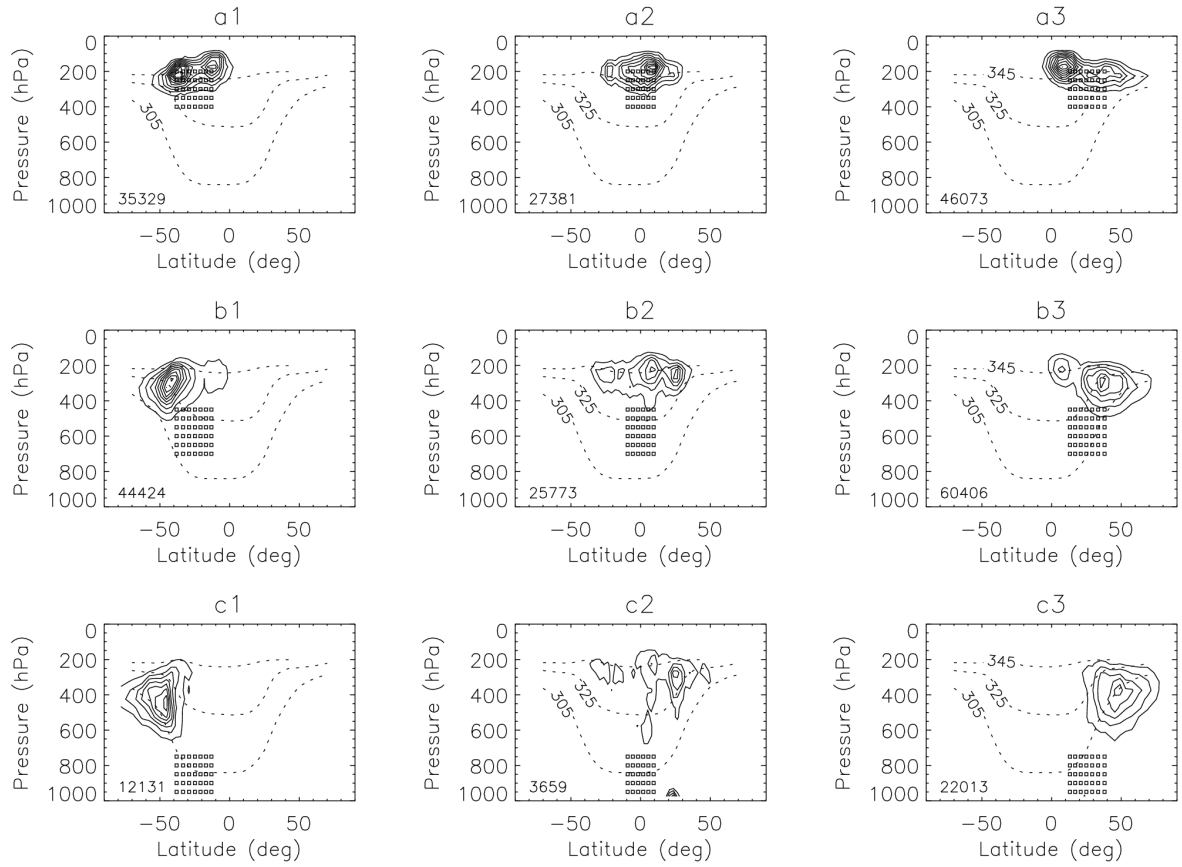

Figure 8: Density of origin for dry air arriving with relative humidity < 20% in the latitude-pressure bands indicated by the grids [see Cau et al. (2007) for details].

number densities to identify the locations of tropical tropopause crossing events, in a search for evidence of the stratospheric fountain. They found that rapid transport from the convectively-mixed portion of the tropical troposphere across the tropical transition zone into the stratosphere (above 380K) was much greater for entry across the bottom of the zone over the west Pacific. Fueglistaler *et al.* (2005) combined this approach with the advection-condensation model to show that the humidity of the stratosphere is strongly influence by the Lagrangian cold point in the west Pacific.

Another key interest in the humidity distribution is the dryness of air across the subtropical troposphere. In cloud free regions, the water vapour has a major influence on the effective brightness temperature of outgoing longwave radiation, and therefore on the ability of the atmosphere to cool to space. The origin of the air contributing to the dry regions would influence the way in which climate could respond to increasing greenhouse gases. Cau *et al.* (2007) calculated back trajectories from a grid spanning the depth of the troposphere between 40S and 40N and used the advection-condensation model of Fig. 6b to find the location of last condensation events. Figure 7b illustrates that the Lagrangian cold point is equally likely to occur at any time along trajectories, while if re-moistening is accounted for the last condensation event is most likely 2-3 days before arrival with a mean of 6 days. Figure 8 depicts the "density of origin" of back trajectories from the grids shown, aggregating the locations of last condensation events over all longitudes and days during one season. Note that dry air in the subtropical lower and mid-troposphere has descended from the extratropics at an average slope steeper than isentropic surfaces owing to an average cooling rate of 1.5 K day^{-1}, consistent with radiative processes.

2.5 Conclusions on Transport

Although the atmosphere is chaotic, making air mass trajectories sensitive to initial conditions, trajectory calculations obtained by interpolation and integration of analyses are remarkably accurate, both in the extratropics and tropics. Illustrations of accuracy include the matching of chemical fingerprints for polluted air masses crossing the entire North Atlantic during the ITCT-Lagrangian aircraft experiment and the ability of reverse domain filling trajectories to reconstruct tracer distributions which have a one-to-one correspondence with observations. Trajectories derived from forecasts are sufficiently accurate to guide aircraft to intercept finescale air masses.

Simple advection-condensation models have been shown to simulate the humidity distribution. These are valuable tools to interrogate re-analyses and general circulation models and to learn about the complex, non-local relationships between the origins of humidity and dry regions and their influence on climate.

3 Balance in the Extratropics

3.1 Geostrophic, hydrostatic and thermal wind balance

In the extratropics, large-scale motions are near to hydrostatic and geostrophic balance. Using the anelastic form of the equations in height coordinates, these balances can be written as:

$$b' = f_0 \frac{\partial \psi_g}{\partial z}, \quad u_g = -\frac{\partial \psi_g}{\partial y}, \quad v_g = \frac{\partial \psi_g}{\partial x} \tag{1}$$

where (u_g, v_g) is the geostrophic wind, f_0 is the Coriolis parameter, (x, y, z) represent the zonal, meridional and vertical coordinates and $b' = g\theta'/\theta_0$ is called buoyancy, θ is potential temperature and g is gravitational acceleration. All three balances are expressed in terms of gradients of *geostrophic streamfunction* which is related to pressure perturbations by $\psi_g = p'/(f_0\rho_r)$ where $\rho_r(z)$ is a reference density.

Taken together they imply *thermal wind balance* which relates the vertical gradients in horizontal wind to the horizontal temperature gradients:

$$f_0 \frac{\partial u_g}{\partial z} = -\frac{\partial b'}{\partial y} \; ; \; f_0 \frac{\partial v_g}{\partial z} = \frac{\partial b'}{\partial x}. \tag{2}$$

3.2 Quasi-geostrophic potential vorticity conservation and inversion

The above balance relations are **diagnostic**, meaning that time derivatives have been neglected so that they cannot predict flow evolution. There are many balance models that consider higher order approximations where time derivatives are retained in some variables. The sense in which they are balanced will be described later. Here we will focus on one balance model, quasi-geostrophic theory, which has formed the cornerstone of concepts in geophysical fluid dynamics.

There are many routes to derive the QG equations (e.g., Vallis 2006; Satoh 2004; Holton 1992). The essential idea is that the atmosphere stays close to geostrophic balance, but that the evolution of the geostrophic variables (vorticity and buoyancy) is related to the **ageostrophic wind components** (u_{ag}, v_{ag}, w) where $u_{ag} = u - u_g$ etc. Defining $\zeta_g = f + \xi_g$ as the vertical component of absolute geostrophic vorticity (planetary plus relative) the curl of the momentum equations gives:

$$\boxed{\text{Vorticity eqn: } D_g \zeta_g = f_0 \tfrac{1}{\rho_r} \tfrac{\partial(\rho_r w)}{\partial z}} \tag{3}$$

$\Longrightarrow$ vortex stretching/contraction increases/decreases absolute vorticity. Conservation of entropy gives:

$$\boxed{\text{Thermodynamic eqn: } D_g b' + N^2 w = 0.} \tag{4}$$

$\Longrightarrow$ advection of reference potential temperature surfaces upwards/downwards results in low/high buoyancy anomalies. Here D_g denotes the geostrophic form of the material derivative given by $D_g = \frac{\partial}{\partial t} + u_g \frac{\partial}{\partial x} + v_g \frac{\partial}{\partial y}$. For example $D_g b'$ means the change in buoyancy seen by an observer following the geostrophic wind.

Both equations contain time-derivatives and terms for the ageostrophic flow (w). We can eliminate w to obtain a prognostic equation for the so-called quasi-geostrophic potential vorticity OR we can eliminate the time-derivatives to obtain a diagnostic equation for w, the so-called Omega equation. Eliminating w from (3) and (4) obtains the QG potential vorticity equation:

$$D_g q = 0 \tag{5}$$

where the QG potential vorticity, q, is defined as

$$\begin{aligned} q &= \zeta_g + \frac{f_0}{\rho_r}\frac{\partial}{\partial z}\left(\frac{\rho_r b'}{N^2}\right) \\ &= \underbrace{f_0 + \beta y}_{f} + \underbrace{\nabla_h^2 \psi_g}_{\xi_g} + \frac{1}{\rho_r}\frac{\partial}{\partial z}\left(\rho_r \frac{f_0^2}{N^2}\frac{\partial \psi_g}{\partial z}\right) \end{aligned} \tag{6}$$

i.e., q is **conserved** following the (geostrophic) flow in the absence of frictional or diabatic effects. (6) involves only derivatives of streamfunction, ψ_g, with coefficients depending only on the reference state $(f_0, N(z), \rho_r(z))$ and can be written as an operator $\mathscr{L}$ acting on streamfunction. In principal this expression can be **inverted** mathematically, given suitable boundary conditions on ψ_g, to obtain:

$$\psi_g = \mathscr{L}^{-1}(q - f)$$

from which geostrophic winds and buoyancy can be calculated (1).

For discussion we can simplify the inversion operator further by making the Boussinesq approximation ($H \ll H_\rho \ll H_\theta$) which implies that ρ_r and N^2 can be considered constants. If we also re-scale the height coordinate such that $\hat{z} = (N/f_0)z$ we find:

$$q' \approx \left(\frac{\partial^2}{\partial x^2} + \frac{\partial^2}{\partial y^2} + \frac{\partial^2}{\partial \hat{z}^2}\right)\psi_g = \hat{\nabla}^2 \psi_g \tag{7}$$

This is a form of Poisson equation and is found in many areas of physics. For example, it is the same relationship as found between a point charge and the electric field potential in electrostatics. Just as a point charge influences other charges far away through the field that it *induces*, a **PV anomaly**, q', influences distant PV anomalies through the streamfunction that it induces there. This principal is called **action-at-a-distance**.

Since there is symmetry between directions in the re-scaled inversion operator, a point PV anomaly far from any boundary influences streamfunction equally in all directions including the vertical and therefore induces anomalies in the buoyancy as well as geostrophic wind. Figure 9 illustrates the induced anomalies for an isolated ball of positive QGPV. Note that the buoyancy gradient, $\frac{\partial b'}{\partial z}$, or perturbation static stability is increased within the +ve PV anomaly and decreased above and below such that the potential temperature surfaces are barely perturbed far away from the PV anomaly. Also there is a cyclonic circulation around the +ve PV anomaly with maximum winds on the edges of the anomaly, decaying with distance outside it. Note that the **natural aspect ratio** of the wind anomalies $\hat{H}/L \sim$

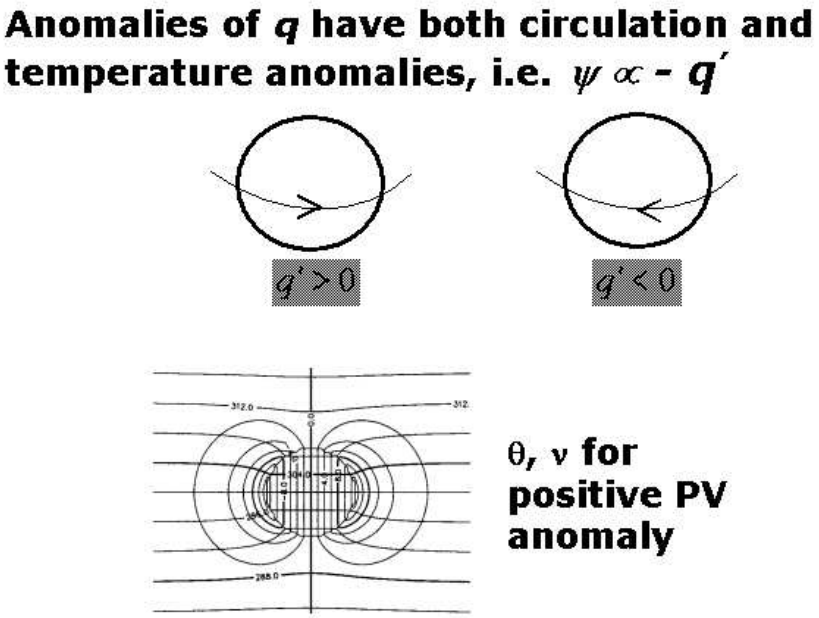

Figure 9: Circulation and deviations of potential temperature surfaces associated with QGPV anomalies.

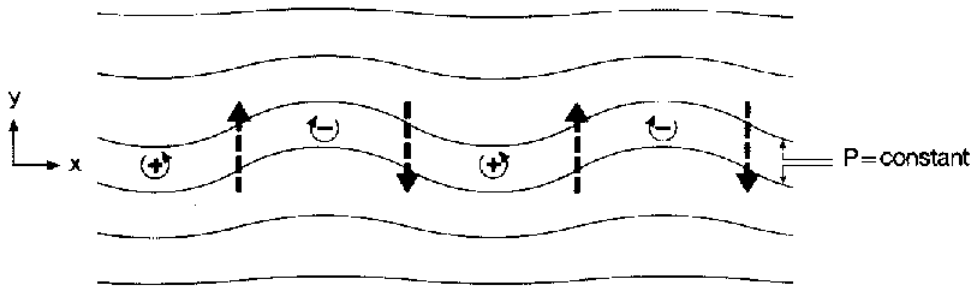

Figure 10: Schematic of a planetary Rossby wave. The + and - signs indicate the centres of PV anomalies due to southward and northward air-parcel displacements across the basic northward PV gradient. The arrows indicate the cyclonic and anticyclonic flow anomalies induced by the PV anomalies, resulting in westward propagation of the wave. [Taken from Hoskins et al. 1985]

1 in the rescaled coordinates or $H/L \sim f_0/N$ in physical coordinates. NH/fL is referred to as the Burger number. QG theory implies that isolated QGPV anomalies induce flows where $Bu \sim 1$ which has implications for the partition between horizontal and vertical motion. In the troposphere $N/f_0 \sim 100$ and therefore we expect wind anomalies to be 100 times as wide as they are deep.

The real power of PV as a diagnostic comes through the combination of conservation with invertibility. This is exemplified by the mechanism for the propagation of Rossby waves – described as waves associated with undulations of PV contours. Consider Fig. 10 showing a wave on a +ve meridional PV gradient. If air is displaced to the south it carries high PV with it, due to material conservation, and forms a +ve PV anomaly. By inversion, this *induces* a cyclonic circulation that will advect air south on the western flank of the +ve anomaly, increasing the anomaly, and return the PV contour towards its undisturbed position on the eastern flank, reducing the anomaly. The net effect is to shift the anomaly towards the west. Try and construct a similar argument for the propagation of the -ve PV anomalies.

The PV perspective also provides a complete description of the growth of wave perturbations on shear flows. For instability (sustained exponential growth) it is necessary to consider two Rossby waves propagating on opposite signed basic state PV gradients. The sign of PV gradient determines the direction of propagation relative to the zonal flow. The condition on opposing PV gradients or more generally propagation directions is called the Charney-Stern necessary criterion for instability (Charney and Stern 1962). It is also essential that the basic state flow is stronger where the PV gradient is positive, so that the self-propagation of the waves acts to oppose the wind shear. This is called the Fjørtoft (1950) criterion for instability. For these reasons the waves are called *counter-propagating Rossby waves* (CRWs). Shear instability was first described in terms of CRWs by Lighthill (1963). Bretherton (1966a) formulated instability precisely in terms of CRWs in a 2-layer model. Later Heifetz *et al.* (2004) showed that the CRW growth mechanism applies to any parallel jet where there are regions of positive and negative cross-stream QGPV gradient.

Shear instability is called **barotropic instability** if it involves interaction between two CRWs on the same horizontal surface, propagating on opposite signed basic state PV gradients. If the CRWs exist at different heights and interact in the vertical, it is called **baroclinic instability** (see Fig. 11). Note that in both cases PV anomalies are formed by horizontal advection of basic state PV gradients - it is the direction of the coupling that differs (Fig. 11).

3.3 PV tracer diagnostics

The two properties of PV that are key to anticipating the evolution from a given initial state are material conservation and its invertibility. The first is far easier to deal with. Ertel PV (as opposed to QGPV - see Holton 1992) is conserved by the unapproximated dynamical equations following adiabatic, frictionless flow. It can be readily calculated from gradients in the prognostic variables of a numerical weather prediction model and then used as a tracer of the flow.

The tracer property can be combined with the reverse domain filling trajectory technique to reveal finescale structure in the atmosphere that can influence the evolution of weather events. For example, Figure 12 shows a the reconstructed PV field in the upper troposphere (300 hPa level) and along a NW-SE vertical section across the upper level trough. The RDF3D technique picks out finescale structure, such as the tropopause fold, which is lost in the gridded analysis.

As illustrated in Fig. 5, the finescale structure has a one to one correspondence with observations which gives us confidence that the trajectories of air masses are simulated with some fidelity. Figure 13 shows the net change in pressure following air masses towards the *arrival grid* (i.e., $p(0) - p(-T)$). Clearly the band of air ahead of the fold (blue) has ascended from the boundary layer to tropopause level within the last 1.75 days (see Fig. 14a for the back trajectories from the X). This *coherent ensemble of trajectories* is used to define *warm conveyor belt (WCB) air masses* (e.g., Wernli and Davies 1997) and is confined in

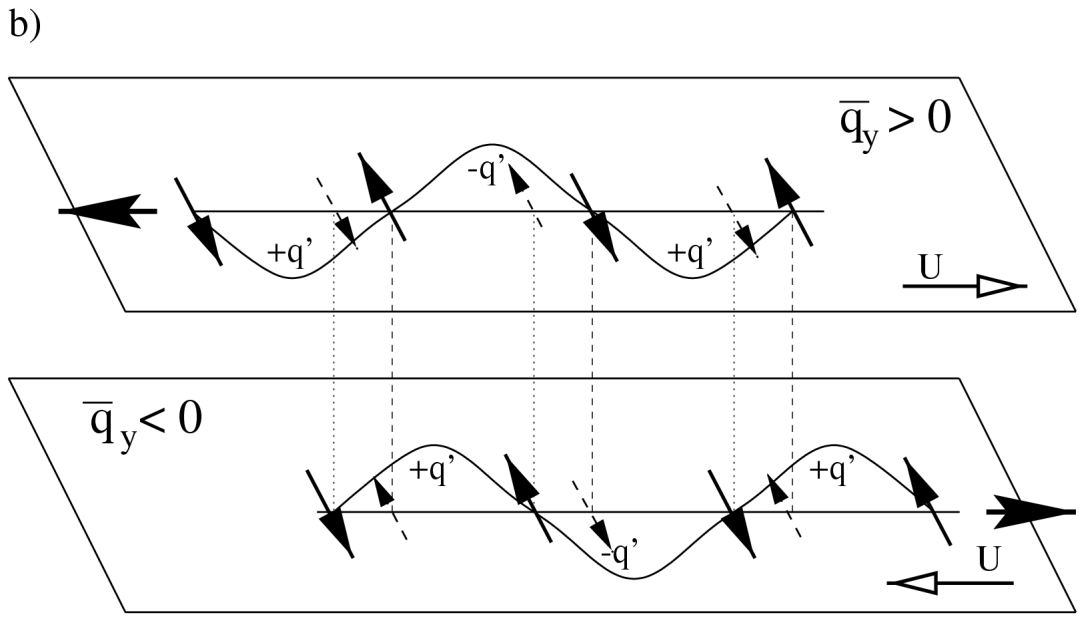

Figure 11: CRWs in baroclinic instability shown in a configuration where interaction enables growth of each CRW but hinders self–propagation. [From Heifetz et al. 2004.]

the vertical too (Fig. 13b). Within WCBs the rapid ascent quickly leads to saturation and precipitation, represented by *large-scale rain* parameterisations in NWP models. The latent heat released can be diagnosed using trajectories too, as seen by the net increase in potential temperature following trajectories (Fig. 14a).

The RDF3D analysis either assumes that tracers are exactly conserved, or examines the net change in analysed variables, irrespective of process. However, a useful way to pick apart the workings of an NWP model is to consider the changes in PV (following air masses) that arise from non-conservative processes associated with each physical parameterisation in a model. Bob Plant (University of Reading) and Peter Clark (Met Office) have developed such a tool in the framework of the Met Office Unified Model. Gray (2006) used the tool to examine the erosion of tropopause folds in simulations.

The full PV conservation equation is written in the form:

$$\frac{Dq}{Dt} = \sum_p S_p \tag{8}$$

where S_p denotes the Lagrangian tendency resulting from one physical process in the model. Tracers q_p are initialised as zero but experience only one of the S_p terms as well as being advected by the model's semi-Lagrangian advection scheme. A passive tracer is also integrated from initial conditions given by the full PV distribution, but with $S = 0$. If the model advection scheme were perfect the method would produce a decomposition of the PV field:

$$q = q_{passive} + \sum_p q_p. \tag{9}$$

In practice the advection scheme results in numerical dissipation and there is a residual in the PV budget with values approximately an order of magnitude smaller than those in the tracer field associated with the strongest processes (such as parameterised convection or large-scale precipitation). Figure 15a shows total PV on an vertical section through a tropopause fold and ascending warm conveyor belt to its east, obtained from a global simulation with 40km grid spacing and a limited area model at 12km. Figure 15b

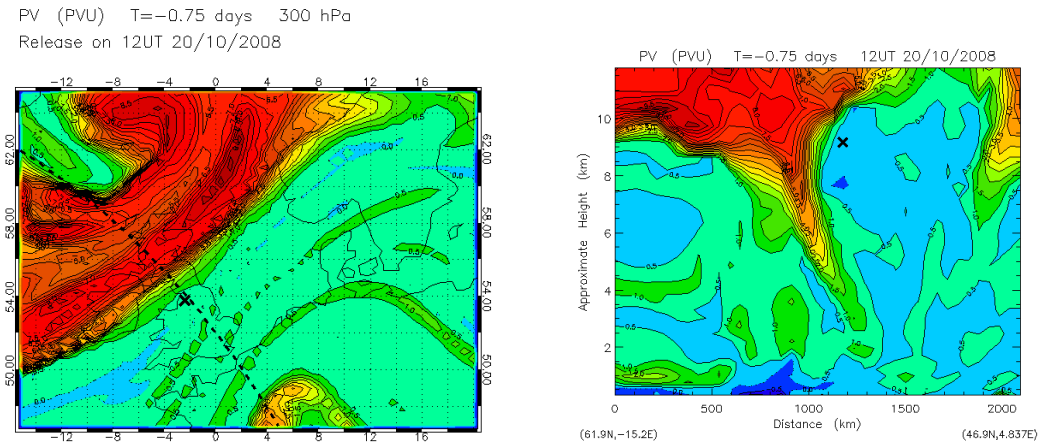

Figure 12: RDF3D reconstructions of the PV field. a) PV on 300 hPa pressure level (interval 0.5 PVU) obtained using back trajectories 0.75 days long. b) Section from NW to SE showing PV.

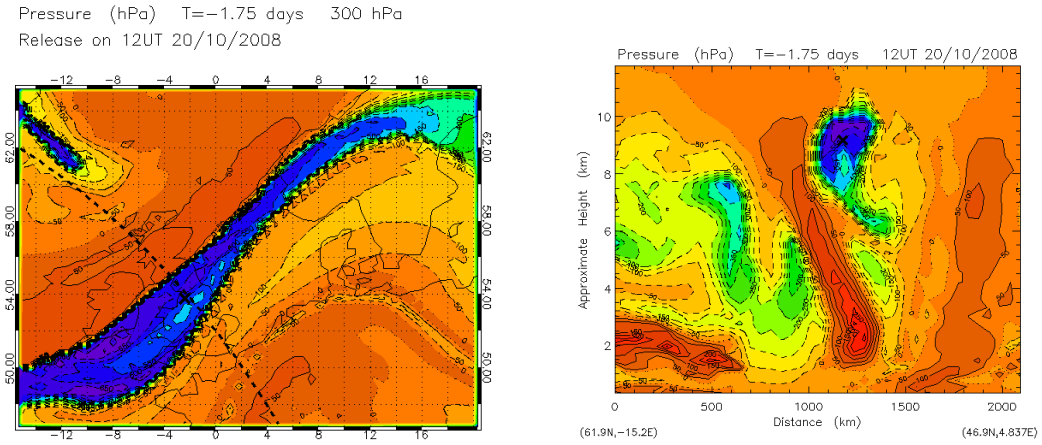

Figure 13: Change in pressure over 1.75 days following air masses to the arrival grid. Blue indicates air that has ascended most. a) Shown at 300 hPa level. b) Along same section as 12b.

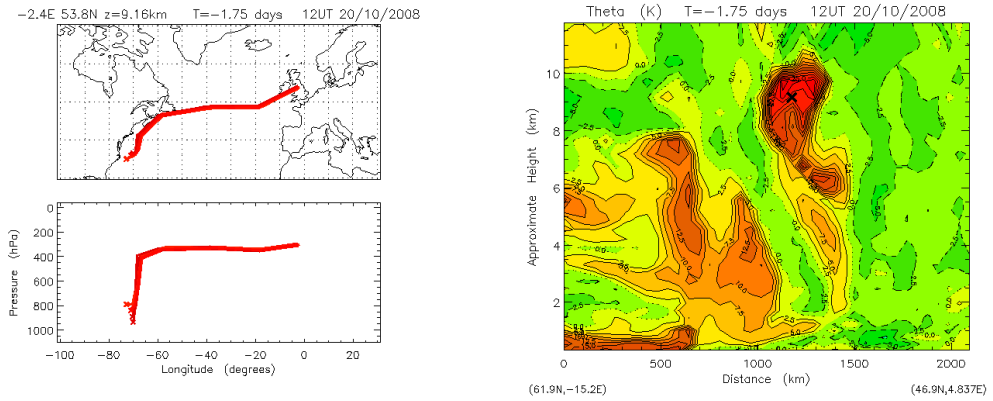

Figure 14: a) Back trajectories from the X on the plans and sections, showing that rapid ascent occurred within a warm conveyor belt (WCB) along East Coast N America. b) Change in potential temperature quantifying heating within the WCB and another WCB ascending over the UK (directly beneath at 4km).

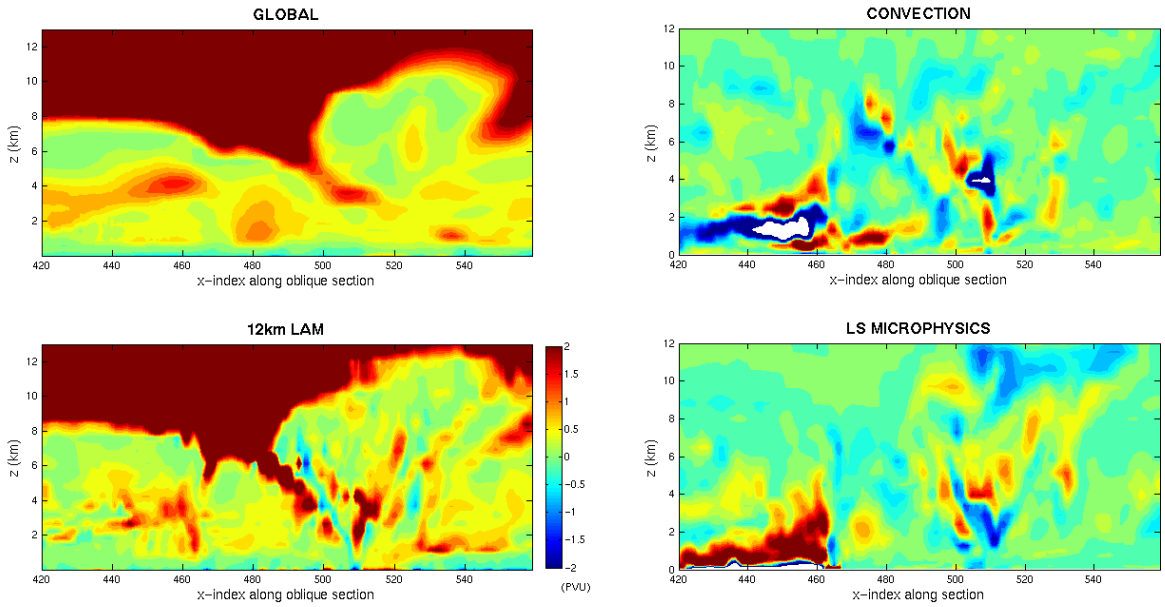

Figure 15: PV from simulations of the Met Office Unified Model. Left) Similar section to Fig. 12b through the global and limited area models. Right) PV tracers from LAM showing accumulated PV change due to convection and large-scale rain parameterisations. [J. Chagnon, U. Reading]

shows two PV tracers which have accumulated non-conservative processes arising from the convection and large-scale precipitation schemes in the limited area model. It is clear that convection results in a negative PV anomaly where the warm conveyor belt reaches the tropopause (the dot) and must contribute to the erosion of the tropopause there. Large-scale rain results in a complex pattern of PV anomalies below. Together they appear to reduce the high PV of the tropopause fold on its eastern flank. It is tempting to associate this behaviour with the difference from the structure seen in the lower resolution global model. However both models are two days into a forecast and so displacement errors in the tropopause trough would be expected and cannot be attributed solely to non-conservative processes.

PV has also been used to diagnosis typical forecast errors in NWP models (e.g., Fehlman and Davies 1997). The World Meteorological Organisation's THORPEX programme is planning a new observational experiment across the Atlantic in 2013 called T-NAWDEX (THORPEX- North Atlantic Waveguide and Downstream Impact Experiment). Its overarching aim will be to investigate in detail the physical processes that are primarily responsible for degradation in 1-7 day forecast skill in global NWP models. PV tracer diagnostics will be a valuable tool to pick apart the evolution of events, the processes acting and identify deficiencies in their representation by the model.

3.4 Piecewise PV inversion (PPVI)

Anomalies in PV are clearly central to the evolution of the balanced flow and phenomena such as Rossby wave propagation, baroclinic instability and extratropical cyclone development. If one believes that a localised PV anomaly structure has been misrepresented by a model, it would be desirable to estimate its consequences for the subsequent evolution. Sophisticated diagnostic tools have been devised to invert the distribution of localised potential vorticity anomalies and infer the flow and static stability anomalies associated with them (Davis and Emanuel 1991; Hakim *et al.* 1996). It is necessary to assume some form of dynamical balance which defines the inversion algorithm - the most basic form of which is

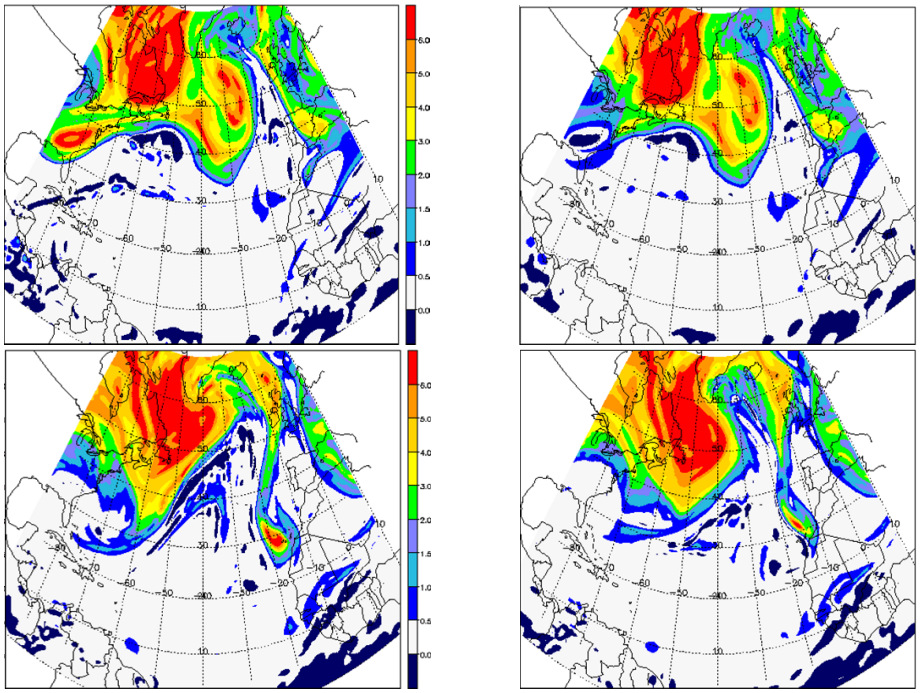

Figure 16: Example of the PPVI technique. Upper row) Initial PV from control (left) and with PV anomaly in SW corner removed. Lower row) 36 hour forecasts from control run and run with initial PV modification. [P. Knippertz, U. Leeds]

quasi-geostrophic balance, although higher order approximations are possible. The technique is called piecewise PV inversion (PPVI). An illustration is given in Fig. 16 where the impact of a PV anomaly in the SW corner of the domain on the downstream development of trough to its east is investigated.

Recently Egger (2008) has criticised the use of PPVI because typically PV anomalies are not isolated features but part of a wave or more complex pattern. Therefore, an arbitrary partition of the domain to isolate a PV feature from its surroundings and then inversion assuming zero surroundings, does not obtain wind fields which would enable prediction of what happens next. Methven and de Vries (2008) suggest that when the PV pattern is wavelike, upper and lower level counter-propagating Rossby wave components can be identified in principal. These would in general be spatially overlapping but orthogonal with respect to wave activity (defined in the next section) such that the evolution of the full flow can be decomposed into simple evolution equations for the propagation of each CRW component and their interactions to obtain phase-locking behaviour and sustained mutual baroclinic growth.

Another technique which gives insights into the effects of forecast model errors is to isolate the PV anomaly associated with an identified misrepresentation of a feature and use PPVI to infer the anomalies in winds and temperature associated with the PV error. These anomalies are then subtracted from the model's prognostic variables and the forecast is re-run. Demirtas and Thorpe (1999) first used satellite imagery in the water vapour channel to identify erroneous structures in PV near the tropopause and then the PPVI technique to examine their consequences for evolution. They went further by using the imagery to create bogus anomalies in an attempt to improve forecasts. However, Swarbrick (2001) showed that on average the impacts on forecast skill were mixed and the procedure is no longer used routinely by the Met Office.

3.5 Conclusions on PV diagnostics

The goal of PV diagnostics is to shed light on the evolution of the balanced flow and its representation in NWP models. They fall into two types:

1. RDF trajectories make use of the approximate material conservation of PV to reconstruct the detailed structure of cyclones and the mesoscale features embedded within them. PV tracers integrated within NWP models take the next step by accumulating the effects of non-conservative processes on PV associated with individual model parameterisations. They reveal the differences between models and attribute them to processes.

2. Piecewise PV inversion can be used as a diagnostic tool to pick apart the non-local influence of features in the flow upon one another. If used judiciously, modification of initial condititions by changing the PV field and associated flow anomalies can shed light on the influences of model error on the subsequent evolution.

There are problems with these techniques, but there is scope for improving them. One major hurdle is an objective means to partition the full flow into a *background state* and the anomalies which develop upon it since the definition of anomaly has such as major influence on inferred impact on evolution. An objective means to partition the PV anomalies into interacting components obeying simple evolution equations has not yet been developed, although De Vries *et al.* (2009) have shown that it is possible for general initial conditions in models with dynamics linearised about zonally symmetric states. Another hurdle is to properly account for the influence of diabatic processes, in particular latent heat release, on the evolution of the anomalies.

4 Mean flow and eddies

4.1 Influence of form of averaging

Rossby waves in the atmosphere are clearly (e.g., Fig. 16) far from the undular limit of small wave slope described by linear theory. Chaotic advection results in the stretching and folding of PV contours, just as with all other tracers. However, PV is still *active* is the sense that it can be inverted, given a suitable balance approximation and boundary conditions, to obtain the flow and temperature fields. Also, in some average sense there is still a "background PV gradient" upon which anomalies propagate and interact. Theories for the evolution of the atmosphere by in large depend on a notional separation of the full flow into a background state and disturbances to it. However, the manner in which the background is extracted has immediate consequences for the diagnosis of its interactions with disturbances. This is the third area central to diagnostics of the extratropics and where much more research effort is required.

Typically people regard "climate" as some form of average which evolves slowly. A time average a fixed locations (grid points) is undesirable since clearly it cannot evolve over the window of interest. Zonal averages (along latitude circles) have serious disadvantages in the presence of large-amplitude waves: the waves form part of the average and cause it to vary rapidly. Since a scale-break in the energy spectra of the atmosphere is not observed (Nastrom and Gage 1985) temporally and spatially filtered states are artificial since they depend on arbitrary decisions on cut-off scales for the averaging filters.

This section focusses on an alternative partition based on global integrals for mass and circulation of particular control volumes. The control volumes are defined by isentropic surfaces (of constant θ) above and below and bounded laterally by PV contours such that higher PV than a threshold $q = Q$ is contained within the volume. If the flow is adiabatic and frictionless, both θ and PV are materially

conserved which implies that there can be no flux of mass across the faces of the volume. Furthermore, Kelvin's circulation theorem shows that the circulation of the volume is also invariant. The *modified Lagrangian mean* state is defined as the zonally symmetric state obtained by *adiabatic re-arrangement* of the full PV distribution, such that it is zonally symmetric but contains the same mass and circulation integrals.

It was first developed by McIntyre (1980) to examine the seasonal evolution of the stratospheric polar vortex and its implications for the ozone hole. In the stratosphere it is a good approximation to assume uniform density in isentropic layers and replace the mass integrals with area integrals. Since there is a direct mapping from the area enclosed by a zonally symmetric PV contour on a sphere and latitude, the background state of chemical constituents in the stratosphere has been diagnosed by associating *equivalent latitudes* with tracer contours on the basis of the area they enclose (Norton 1994; Lary *et al.* 1995). The great conceptual advantage of the MLM state is that it is inherently slowly evolving since it can only change through non-conservative processes which are weak on average compared with advection.

4.2 Vortex erosion process

When Rossby waves propagating on the PV gradient break, mass is advected away from the vortex edge in high PV filaments. Figure 17 shows an example from an idealised single layer QG global simulation. The PV filaments are stretched and thinned by chaotic advection. On average filaments thin at an exponential rate until they are narrow enough to be mixed away by small-scale turbulence. The net result is that the mass between PV contours bounding the vortex edge regions decreases (and mass in the low PV region increases). This results in a tighter PV gradient and inversion implies that the jet around the vortex edge is stronger. This behaviour is clear in the evolution of the MLM state PV, shown in the right panel versus equivalent latitude and time. Note that it takes 50 days for the MLM PV gradient to tighten despite rapid stirring and eddy formation. In summary, the irreversible deformation of PV contours by wave breaking and inevitable dissipation at small scales has accelerated the vortex jet but decreased the mass enclosed. This is called the *vortex erosion process*. Its rate is independent of the details of small-scale dissipation, but depends on the wave breaking and stirring behaviour (Legras and Dritschel 1993). Ambaum (1997) argued that a similar process results in the sharpening of the tropopause on isentropic surfaces that intersect it.

Crucially, the stronger PV gradient implies a stronger restoring mechanism for Rossby waves (the "Rossby elasticity"), making wave breaking more difficult to achieve. In this way, a sharp vortex edge is a robust phenomenon: strengthened when PV gradients are weak and undular when PV gradients are strong (Haynes *et al.* 2001). A vortex edge characterised by a step change in PV even provides a barrier to a propagating vortex dipole directed at it, provided that the vorticity of the dipole is less than that of the vortex edge (Dritschel and McInytre 2007). It is very difficult to break the PV contours around the vortex edge, inhibiting exchange of mass between the vortex interior and its surroundings. Therefore the edge is referred to as a *transport barrier*.

In the troposphere and especially across the tropopause it is a poor approximation to assume that the isentropic density is uniform. In this case, the MLM state can still be obtained through adiabatic re-arrangement, but the equivalent latitudes need to be found such that the mass and circulation constraints are simultaneously obeyed. Figure 18 shows recent results from such a calculation (Methven and Berrisford, paper in preparation). Areas enclosed by PV contours are used as the first guess for equivalent latitudes, the zonally symmetric MLM state is inverted (using a 2D inverter on the sphere) and the inconsistency between the zonal wind obtained and the circulation integrals is used to iterate the equivalent latitudes. The result is a background PV distribution defined by equivalent-latitude and isentropic coordinates and the corresponding zonal flow (and density) obtained by PV inversion. Note how both evolve slowly. Periods where the PV gradient at the tropopause shifts slowly towards the pole are related to Rossby wave breaking and ejection of filaments.

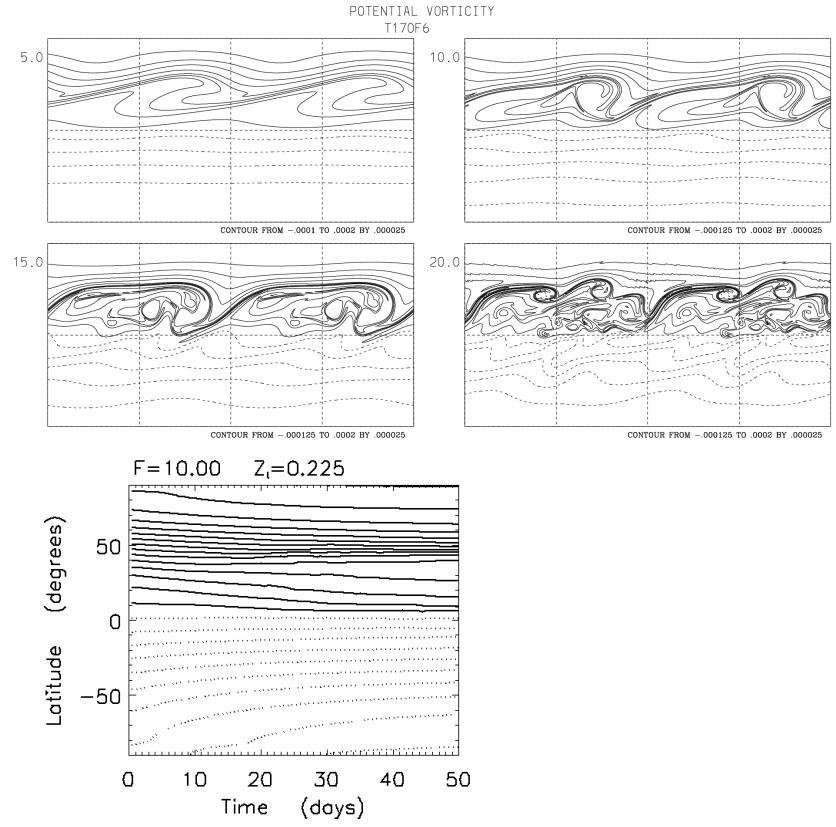

Figure 17: Left: QG single layer global simulation of a Rossby wave critical layer forced by orography (zonal wavenumber 2). QGPV contours shown on cylindrical map projection. Right: Evolution of background state obtained by re-arranging PV to be zonally symmetric while preserving mass between PV contours. [from Methven (2003)]

.

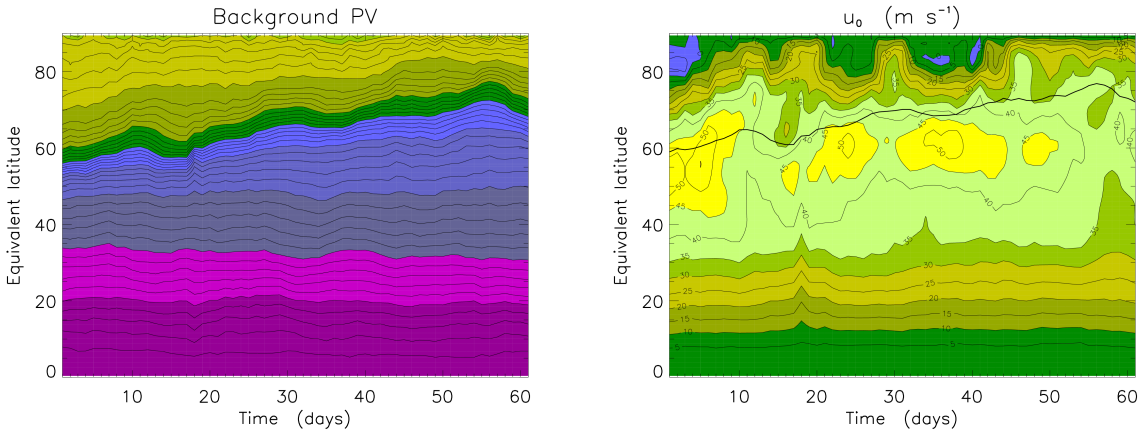

Figure 18: Modified Lagrangian Mean state obtained from ERA-Interim analyses for June and July 2007. a) PV on 320K isentropic surface. b) Zonal flow obtained by PV inversion.

4.3 Wave activity conservation

Existing theory on Rossby wave breaking behaviour and its effects on the background flow are hinged on the conservation of **wave activity**, also known as pseudomomentum (Andrews and McIntyre 1976). For simplicity, we will derive the wave activity conservation law for small amplitude Rossby waves. Multiplying the QGPV equation by q' we obtain:

$$\frac{1}{2}\frac{\partial}{\partial t}\left(q'^2\right)+\frac{\overline{u}}{2}\frac{\partial}{\partial x}\left(q'^2\right)+v'q'\frac{\partial \overline{q}}{\partial y}=0 \tag{10}$$

Taking the zonal average eliminates the term with the x-derivative giving:

$$\begin{aligned}\frac{\partial}{\partial t}\left(\frac{1}{2}\frac{q'^2}{\overline{q}_y}\right)+\overline{v'q'} &= 0\\ \frac{\partial A}{\partial t}+\nabla.\mathbf{F} &= 0\end{aligned} \tag{11}$$

where the quantity in the time derivative, A, is called wave activity density and $\mathbf{F}=(-\overline{u'v'},\ \overline{v'b'}f_0/N^2)$ is called the Eliassen-Palm (EP) flux (Eliassen and Palm 1961). The relation $\overline{v'q'}=\nabla.\mathbf{F}$ is called the Taylor identity and was derived for 2D barotropic dynamics by Taylor (1915) and in this 3D QG setting by Bretherton (1966b).

Note that if a zonally symmetric PV contour is displaced meridionally by distance η, the PV anomaly of the displaced air relative to its surroundings at the new latitude is $q'=-\eta\overline{q}_y$. Therefore, wave activity is related to the square of air parcel displacements associated with disturbances to a background state. It turns out that Eqn.(11) applies to large-amplitude waves, although the expressions for the density A and flux $\mathbf{F}$ must be modified to account for large displacements (Andrews and McIntyre (1978); McIntyre and Shepherd (1987)). The equation is in the form of a global conservation law which Haynes (1988) showed is valid for the primitive equations on the sphere. However, the conservation law is only valid for large-amplitude disturbances if the background state is defined by the Modified Lagrangian Mean.

Since the MLM state cannot be changed directly by adiabatic eddy fluxes, $\nabla.\mathbf{F}$ cannot affect it. This is a major conceptual departure from the more familiar zonal mean (Eulerian) framework where the divergence of EP flux associated with adiabatic eddy motions "forces" an acceleration in zonal mean zonal wind. Instead one must regard the adiabatic eddy motions as stirring the flow, causing irreversible deformation of PV contours by Rossby wave breaking, such that the non-conservative mixing of PV filaments is inevitable - a manifestation of the vortex erosion process.

4.4 Rossby wave packets and teleconnections

Under certain conditions the EP flux is related to the group velocity of Rossby wave packets (Hayes 1977; Edmon *et al.* 1980) by:

$$\mathbf{F}=\mathbf{c}_g A \tag{12}$$

See Vallis (2006), Sec. 7.2.2 for a proof. Therefore, wave activity density increases where Rossby wave packets converge ($\nabla.\mathbf{F}<0$). This is the situation at a Rossby wave critical layer, where the flow speed matches the wave phase speed. Hoskins and Karoly (1981) showed that it is possible to calculate the paths of Rossby wave packets using atmospheric model data and the **ray tracing** technique. This technique assumes that the background through which the waves propagate varies slowly compared with the phase of the wave (e.g., Andrews *et al.* (1987), App. 4A). Although this is not strictly valid for the

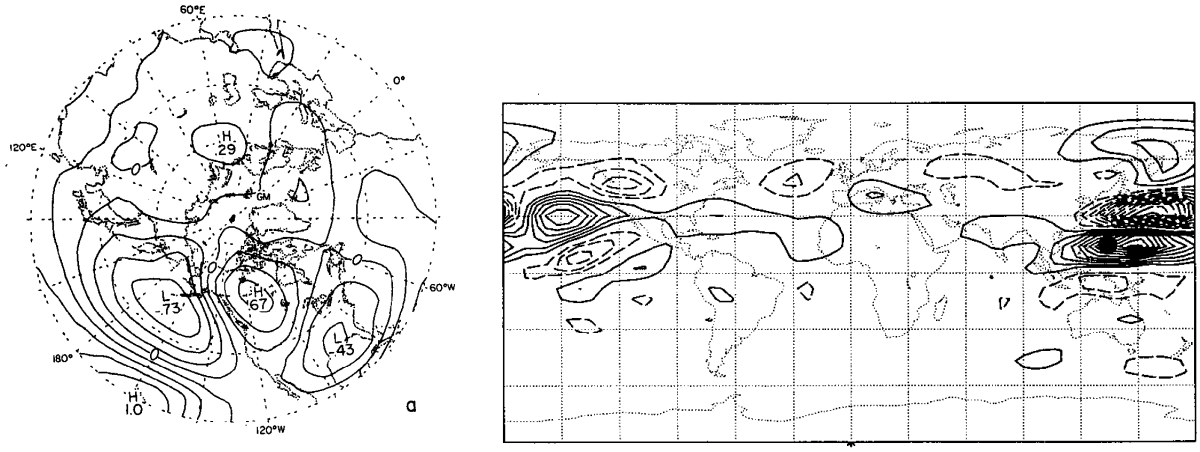

Figure 19: Left: Wallace and Gutzler (1981) identified the PNA pattern with the map of correlation coefficient between time series of 500 hPa geopotential height at the point 20N, 160W and every other location. Right: Barotropic model vorticity response to forcing at 15N, 135E resembles the PNA pattern outside the W. Pacific (Hoskins and Ambrizzi 1993).

atmosphere, the ray paths obtained bear close resemblance to the Rossby wave trains that are frequently observed in the atmosphere.

Probably the most prominent example is the Pacific North American (PNA) pattern which can be related to a stationary Rossby wave emanating from the tropical Pacific and extending across North America along a great circle Wallace and Gutzler 1981. It is believed to be an upper tropospheric Rossby wave response to forcing by heating in the tropics. The pattern occurs so frequently with similar phase between positive and negative vorticity anomalies that it appears as a leading pattern of atmospheric variability. Patterns diagnosed using correlation statistics on atmospheric data are typically called **teleconnection patterns** (see Wallace and Hobbs (2006)). They highlight the propagation of a signal from a wave source to remote regions where it can perturb the atmosphere and even alter the background state. Sardeshmukh and Hoskins (1988) derived an expression for the "source" of Rossby wave activity associated with divergent flow in the upper troposphere. There has been a boost in research activity in Rossby wave trains and tropical forcing by Rossby wave sources, prompted by some particularly anomalous seasons across Europe that have been associated with persistent Rossby wave patterns.

4.5 Coherent structures: Cyclone tracking

Rossby waves in the atmosphere are frequently "large-amplitude" in the sense that the wave-slope of PV contours is greater than unity. Rossby wave breaking results in the over-turning of PV contours and the formation of coherent structures which can often persist for many days. One manifestation of this behaviour is the mature extratropical cyclone where PV contours and low level θ hook around the cyclone centre and it develops into a coherent vortex as opposed to open wave. The structural changes in weather systems as they develop make them difficult to characterise statistically. The earliest measures of stormtrack variability concentrated on the variance of band-pass filtered fields such as geopotential height or vorticity. It is not possible to ascribe the variance statistics to particular phenomena. Alternatively, authors have identified coherent vortices (e.g., as maxima in relative vorticity) and track them across a sequence of analyses (e.g., Hoskins and Hodges 2002). The advantage of this approach is that the tracks of the storms give information on communication between regions of the atmosphere, as well as the influence of aggregate statistics of storms on variability (20).

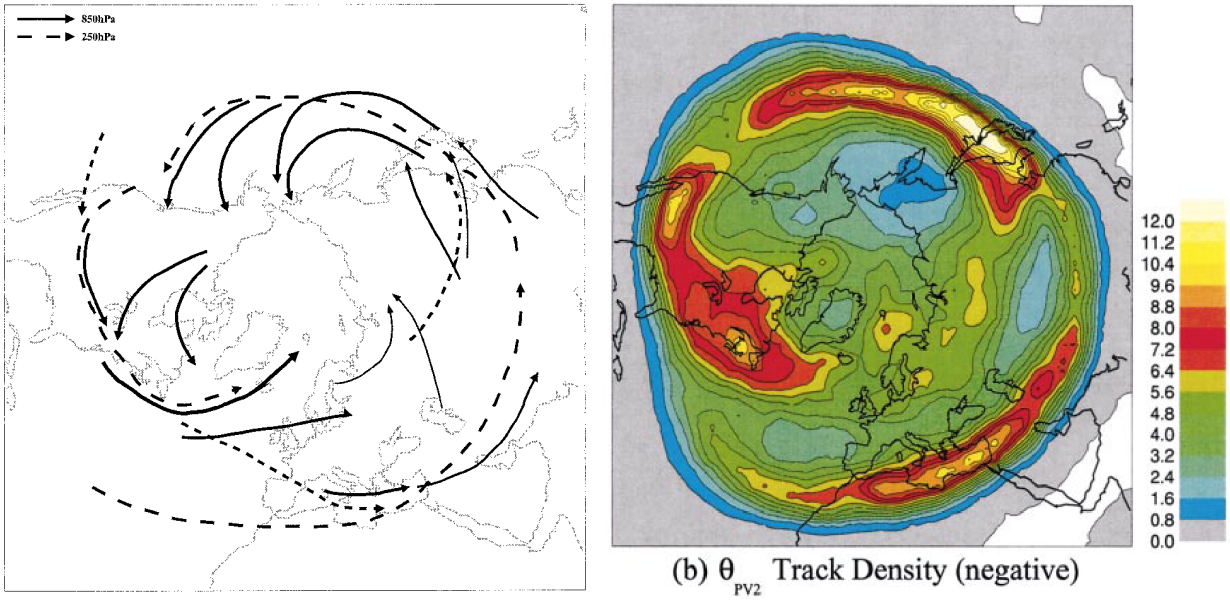

Figure 20: Cyclone tracking [from Hoskins and Hodges 2002]. a) Synthesis of average tracks in the lower (solid) and upper (dashed) troposphere. b) Density of tracks of cold anomalies on the tropopause (θ on 2PVU surface).

Work on track statistics is developing rapidly. For example, Catto, Shaffrey and Hodges (submitted) have built up storm composites by identifying the centre and direction of motion of a cyclone at its maximum intensity (in vorticity) and averaging many storms in a frame of reference where the cyclone centre is at the origin and the storm is rotated such that right is its direction of motion. They have used this technique to investigate the differences in storms from atmospheric analyses and those simulated by climate models.

Froude *et al.* (2007) have used the cyclone tracking algorithn of Hodges (1996) to diagnose systematic differences between the forecasts of cyclones from different operational centres (ECMWF and NCEP). The comparison between centres has been facilitated greatly by the construction of the TIGGE (THORPEX Interactive Grand Global Ensemble) database which archives operational ensemble forecasts for 10 global forecasting centres. Froude (2010, accepted by *Weather and Forecasting*) compare the statistics of storms from each forecast centre versus lead time. Figure 21a shows that many centres underestimate the intensity of extratropical cyclones, especially at longer lead times. This may be associated with effects of model resolution or differences numerical dissipation or maybe more complex than this. Further investigation to pin differences down to the formulation of models or parameterisation of physical processes would be a fruitful avenue of research. One approach would be to use the PV tracer diagnostics. Figure 21b also shows that all centres underestimate the speed of coherent features. Once possibility is that the background flow at the steering level of the cyclones is too weak, although there are many complications making interpretation difficult: once baroclinic waves reach large amplitude and start wrapping up nonlinearly how is phase speed defined and can the relevant background state be pin-pointed?

4.6 Conclusions on wave activity and cyclone tracking

Large-scale waves in the atmosphere are manifestly large-amplitude in nature, exhibiting wave breaking behaviour and the formation of coherent structures such as mature extratropical cyclones. Theory is insuffiently advanced to provide a diagnostic toolkit to describe flow of this nature. Frequently, diag-

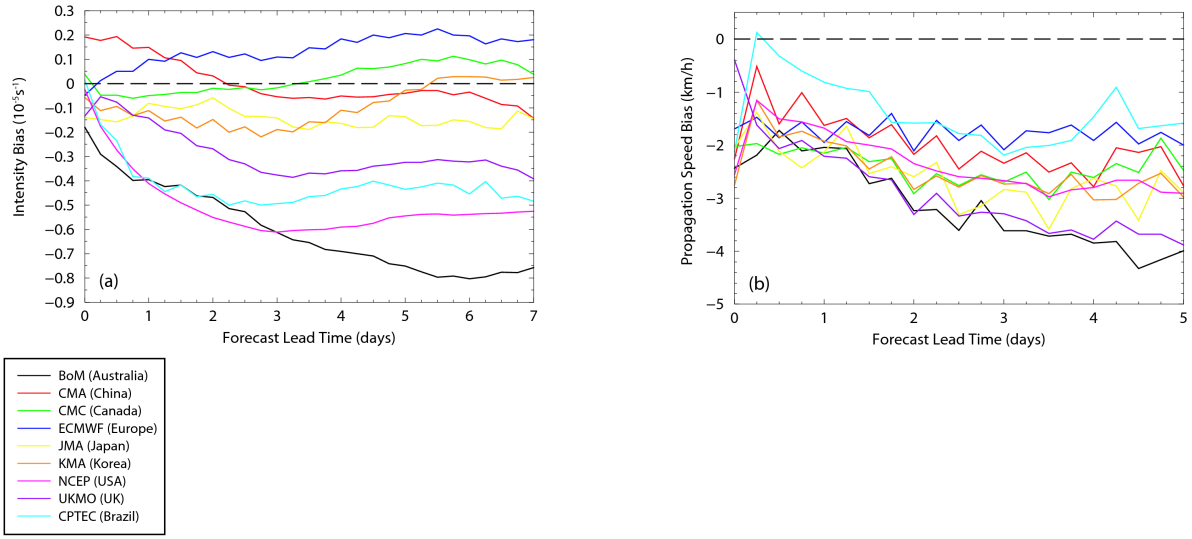

Figure 21: Statistics of cyclones tracked in forecasts from 9 centres contributing to the TIGGE database. [Froude, 2010, accepted by Weather and Forecasting].

nostics are applied directly from the linear theory of undular waves (with small wave slope) or in the tracking of isolated coherent vortices. More research is needed to bring the two views closer to one another in the quantitative diagnosis of "wave-mean flow interaction". This talk has focussed on one particular approach which appears promising: it revolves around the definition of a zonally symmetric background state obtained by adiabatic re-arrangement of PV contours - the modified Lagrangian mean state. The advantages of this framework are that no scale-separation or averaging filter is applied and that the background can only evolve through non-conservative processes. Thus global constraints are built into the definition of the background and as a result it is inherently slowly varying.

5 Conclusions

Three main discussion threads have been drawn together in order to address the influence of non-local behaviour of atmospheric dynamics on the design of diagnostics. The non-local nature is related to: i) advective transport of long-lived tracers, ii) action-at-a-distance associated with potential vorticity inversion and phenomena such as coherent vortices and iii) the remote effects of partitioning the full flow into a background flow (or climate) and disturbances to it. All three are of paramount importance for both weather forecasting and climate change simulation. The common theme emerging is the diagnosis of the atmosphere from a Lagrangian frame of reference; considering the trajectories of fluid parcels. It is obviously advantageous for tracer transport by construction. The advantages for the evolution of waves and vortices come through the approximate material conservation of PV, such that it behaves as a dynamically-active tracer. The third thread was also linked by defining the background state in terms of the modified Lagrangian mean, since it is constructed from the PV distribution while simultaneously respecting the global constraints of mass and circulation conservation. This is a fertile area for exploration, since many of the theoretical tools have only been developed in recent decades but their application to real flows is difficult and requires careful design of novel diagnostics.

Acknowledgements

Many thanks to the people who contributed their ideas and figures for this talk. In particular, Mike Blackburn, Michelle Cain, Jen Catto, Jeffrey Chagnon, Lizzie Froude and Len Shaffrey from Reading and Peter Knippertz (Leeds). Most of the ideas have been formulated over many years of interesting discussions in the Dynamical Processes Group in the Department of Meteolorology especially with Brian Hoskins, Mike Blackburn, Kevin Hodges, Maarten Ambaum, Hylke de Vries and Tom Frame.

References

Ambaum, M. (1997). Isentropic formation of the tropopause. *J. Atmos. Sci.*, **54**, 555–568.

Andrews, D. and McIntyre, M. (1976). Planetary waves in horizontal and vertical shear: The generalized Eliassen-Palm relation and the mean zonal acceleration. *J. Atmos. Sci.*, **33**, 2031–2048.

Andrews, D. and McIntyre, M. (1978). An exact theory of nonlinear waves on a Lagrangian-mean flow. *J. Fluid Mech.*, **89**, 609–646.

Andrews, D., Holton, J., and Leovy, C. (1987). *Middle atmosphere dynamics*. Academic Press. 489 pp.

Arnold, S., Methven, J., Evans, M., Chipperfield, M., Lewis, A., Hopkins, J., McQuaid, J., Watson, N., Purvis, R., Lee, J., Atlas, E., Blake, D., and Rappenglück, B. (2007). Statistical inference of OH concentrations and air mass dilution rates from successive observations of non-methane hydrocarbons in single air masses. *J. Geophys. Res.*, **112**, D10S40, doi:10.1029/2006JD007594.

Balluch, M. and Haynes, P. (1997). Quantification of lower stratospheric mixing processes using aircraft data. *J. Geophys. Res.*, **102**, 23487–23504.

Bretherton, F. (1966a). Baroclinic instability and the short wavelength cut-off in terms of potential vorticity. *Q. J. R. Meteorol. Soc.*, **92**, 335–345.

Bretherton, F. (1966b). Critical layer instability in baroclinic flows. *Q. J. R. Meteorol. Soc.*, **92**, 325–334.

Cau, P., Methven, J., and Hoskins, B. (2005). Representation of dry tropical layers and their origins in ERA-40 data. *J. Geophys. Res.*, **110, D06110**, doi:10.1029/2004JD004928.

Cau, P., Methven, J., and Hoskins, B. (2007). Origins of dry air in the tropics and subtropics. *J. Climate*, **20**, 2745–2759.

Charney, J. and Stern, M. (1962). On the stability of internal baroclinic jets in a rotating atmosphere. *J. Atmos. Sci.*, **19**, 159–172.

Davis, C. and Emanuel, K. (1991). Potential vorticity diagnostics of cyclogenesis. *Mon. Weather Rev.*, **119**, 1929–1953.

De Vries, H., Methven, J., Frame, T., and Hoskins, B. (2009). An interpretation of baroclinic initial value problems: Results for simple basic states with nonzero interior PV gradients. *J. Atmos. Sci.*, **66**, 864–882.

Demirtas, M. and Thorpe, A. (1999). Sensitivity of short-range forecasts to local potential vorticity modifications. *Mon. Weather Rev.*, **127**, 922–939.

Dritschel, D. and McInytre, M. (2007). Multiple jets as PV staircases: the Phillips effect and the resilience of eddy-transport barriers. *J. Atmos. Sci.*, page In Press.

Edmon, H., Hoskins, B., and McIntyre, M. (1980). Eliassen-Palm cross-sections for the troposphere. *J. Atmos. Sci.*, **37**, 2600–2616.

Egger, J. (2008). Piecewise potential vorticity inversion: Elementary tests. *J. Atmos. Sci.*, **65**, 2015–2024.

Eliassen, A. and Palm, E. (1961). On the transfer of energy in stationary mountain waves. *Geofys. Publ.*, **22**, 1–23.

Fehlman, R. and Davies, H. (1997). Misforecasts of synoptic systems: Diagnosis via PV retrodiction. *Mon. Weather Rev.*, **125**, 2247–2264.

Fehsenfeld, F. (2006). ICARTT overview. *J. Geophys. Res.*, page this volume.

Fjørtoft, R. (1950). Application of integral theorems in deriving criteria of stability for laminar flows and for the baroclinic circular vortex. *Geofys. Publ.*, **17**, No. 6, 1–52.

Froude, L., Bengtsson, L., and Hodges, K. (2007). The prediction of extratropical storm tracks by the ECMWF and NCEP ensemble prediction systems. *Mon. Weather Rev.*, **135**, 2545–256.

Fueglistaler, S., Bonazzola, M., Haynes, P., and Peter, T. (2005). Stratospheric water vapor predicted from the Lagrangian temperature history of air entering the stratosphere in the tropics. *J. Geophys. Res.*, **110**, doi:10.1029/2004JD005516.

Gray, S. (2006). Mechanisms of midlatitude cross-tropopause transport using a potential vorticity budget approach. *J. Geophys. Res.*, **111**, D17113, doi:10.1029/2005JD006529.

Hakim, G., Keyser, D., and Bosart, L. (1996). The Ohio Valley wave-merger cyclogenesis event of 25-26 January 1978. Part II: Diagnosis using quasigeostrophic potential vorticity inversion. *J. Atmos. Sci.*, **124**, 2176–2205.

Hayes, M. (1977). A note on group velocity. *Proc.Roy.Soc.London*, **354**, 533–535.

Haynes, P. (1988). Forced, dissipative generalisations of finite-amplitude wave-activity conservation relations for zonal and non-zonal basic flows. *J. Atmos. Sci.*, **45**, 2352–2362.

Haynes, P., Scinocca, J., and Greenslade, M. (2001). Formation and maintenance of the extratropical tropopause by baroclinic eddies. *Geophys. Res. Lett.*, **28**, 4179–4182.

Heifetz, E., Bishop, C., Hoskins, B., and Methven, J. (2004). The counter-propagating Rossby wave perspective on baroclinic instability. Part I: Mathematical basis. *Q. J. R. Meteorol. Soc.*, **130**, 211–231.

Hodges, K. (1996). Spherical nonparametric estimators applied to the UGAMP model integration for AMIP. *Mon. Weather Rev.*, **124**, 2914–2932.

Holton, J. (1992). *An introduction to dynamic meteorology*. Academic Press.

Hoskins, B. and Ambrizzi, T. (1993). Rossby wave propagation on a realistic longitudinally varying flow. *J. Atmos. Sci.*, **50**, 1661–1671.

Hoskins, B. and Hodges, K. (2002). New perspectives on the Northern Hemisphere winter storm tracks. *J. Atmos. Sci.*, **59**, 1041–1061.

Hoskins, B. and Karoly, D. (1981). The steady linear response of a spherical atmosphere to thermal and orographic forcing. *J. Atmos. Sci.*, **38**, 1179–1196.

Hoskins, B., McIntyre, M., and Robertson, A. (1985). On the use and significance of isentropic PV maps. *Q. J. R. Meteorol. Soc.*, **111**, 877–946.

Jackson, D., Methven, J., and Pope, V. (2001). Transport in the low latitude tropopause zone diagnosed using particle trajectories. *J. Atmos. Sci.*, **58**, 173–192.

Lary, D., Chipperfield, M., Pyle, J., Norton, W., and Riishøjgaard, L. (1995). Three-dimensional tracer initialization and general diagnostics using equivalent PV latitude–potential temperature coordinates. *Q. J. R. Meteorol. Soc.*, **121**, 187–210.

Legras, B. and Dritschel, D. (1993). Vortex stripping and the generation of high vorticity gradients in 2-D flows. *Appl. Sci. Res.*, **51**, 445–455.

Lighthill, M. (1963). Boundary layer theory. In L. Rosenhead, editor, *Laminar boundary layers*, pages 46–113. Oxford U Press.

McIntyre, M. (1980). Towards a Lagrangian-mean description of stratospheric circulations and chemical transports. *Phil. Trans. R. Soc. Lond.*, **A296**, 129–148.

McIntyre, M. and Shepherd, T. (1987). An exact local conservation theorem for finite-amplitude disturbances to non-parallel shear flows, with remarks on Hamiltonian structure and on Arnol'd's stability theorems. *J. Fluid Mech.*, **181**, 527–565.

Methven, J. (2003). The influence of PV inversion on polar vortex dynamics and passive tracer simulations in atmosphere-like regimes. *Q. J. R. Meteorol. Soc.*, **129**, 1191–1215.

Methven, J. and de Vries, H. (2008). Comments on "Piecewise Potential Vorticity Inversion: Elementary tests. *J. Atmos. Sci.*, **65**, 3003–3008.

Methven, J. and Hoskins, B. (1999). The advection of high resolution tracers by low resolution winds. *J. Atmos. Sci.*, **56**, 3262–3285.

Methven, J., Arnold, S., O'Connor, F., Barjat, H., Dewey, K., Kent, J., and Brough, N. (2003). Estimating photochemically produced ozone throughout a domain using flight data and a Lagrangian model. *J. Geophys. Res.*, **108(D9)**, 4271, doi:10.1029/2002JD002955.

Methven, J., Arnold, S., Stohl, A., Evans, M., Avery, M., Law, K., Lewis, A., Monks, P., Parrish, D., Reeves, C., Schlager, H., Atlas, E., Blake, D., Coe, H., Crosier, J., Flocke, F., Holloway, J., Hopkins, J., McQuaid, J., Purvis, R., Rappengluck, B., Singh, H., Watson, N., Whalley, L., and Williams, P. (2006). Establishing Lagrangian connections between observations within air masses crossing the Atlantic during the ICARTT experiment. *J. Geophys. Res.*, **111**, D23S62, doi:10.1029/2006JD007540.

Nastrom, G. and Gage, K. (1985). A climatology of atmospheric wavenumber spectra of wind and temperature observed by commercial aircraft. *J. Atmos. Sci.*, **42**, 950–960.

Newell, R. and Gould-Stewart, S. (1981). A stratospheric fountain? *J. Atmos. Sci.*, **38**, 2789–2796.

Norton, W. (1994). Breaking Rossby waves in a model stratosphere diagnosed by a vortex-following coordinate system and a technique for advecting material contours. *J. Atmos. Sci.*, **51**, 654–673.

Pierrehumbert, R. and Roca, R. (1998). Evidence for control of Atlantic subtropical humidity by large scale advection. *Geophys. Res. Lett.*, **25**, 4537–4540.

Sardeshmukh, P. and Hoskins, B. (1988). Generation of global rotational flow by steady idealized tropical divergence. *J. Atmos. Sci.*, **45**, 1228–1251.

Satoh, M. (2004). *Atmospheric circulation dynamics and general circulation models*. Springer. pp.643.

Sherwood, S. (1996). Maintenance of the free-tropospheric tropical water vapor budget distribution. Part II: Simulation by large-scale advection. *J. Climate*, **9**, 2919–2934.

Sutton, R., MacLean, H., Swinbank, R., and O'Neill, A. (1994). High-resolution stratospheric tracer fields estimated from satellite observations using Lagrangian trajectory calculations. *J. Atmos. Sci.*, **51**, 2995–3005.

Swarbrick, S. (2001). Applying the relationship between potential vorticity fields and water vapour imagery to adjust initial conditions in NWP. *Meteorol. Apps.*, **8**, 221–228.

Taylor, G. (1915). Eddy motion in the atmosphere. *Phil. Trans. Soc. Lond.*, **A215**, 1–23.

Vallis, G. (2006). *Atmospheric and oceanic fluid dynamics*. Cambridge University Press. 745pp.

Wallace, J. and Gutzler, D. (1981). Teleconnections in the geopotential height field during Northern Hemisphere winter. *Mon. Weather Rev.*, **109**, 784–812.

Wallace, J. and Hobbs, P. (2006). *Atmospheric Science: An introductory survey*. Academic Press. 483pp.

Wernli, H. and Davies, H. (1997). A Lagrangian based analysis of extratropical cyclones. I: The method and some applications. *Q. J. R. Meteorol. Soc.*, **123**, 467–489.